Roy Featherstone

Department of Systems Engineering
Australian National University
Canberra ACT 0200, Australia

An Empirical Study of the Joint Space Inertia Matrix

Abstract

The joint-space inertia matrix of a robot mechanism can be highly ill-conditioned. This phenomenon is not merely a numerical artifact; it is symptomatic of an underlying property of the mechanism itself that can make it more difficult to simulate or control. This paper investigates the problem by means of an empirical study of the eigenvalues, eigenvectors and condition number of the joint-space inertia matrix. It is shown that the condition number is typically large, and that it grows anywhere from $O(N)$ to $O(N^4)$ with the number of bodies in the system. Several graphs are presented, showing how the condition number varies with configuration, the number of links, variations in link sizes, variations in connectivity, and fixed or floating bases. Explanations are offered for some of the observed effects.

KEY WORDS—robot dynamics, rigid body dynamics, inertia matrix, mass matrix, condition number, ill-conditioning

1. Introduction

The joint-space inertia matrix (JSIM) plays an important role in the simulation and control of robot mechanisms. It is well known that the JSIM is both symmetric and positive-definite, but it can also be highly ill-conditioned. This property is not merely a numerical artifact; it is symptomatic of an underlying ill-conditioning phenomenon in the mechanism itself. Thus, an ill-conditioned JSIM is a useful predictor of a loss of accuracy in forward and inverse dynamics calculations, even if those calculations do not involve the JSIM directly, and it suggests that the mechanism itself may be intrinsically more difficult to control.

This paper investigates the nature and magnitude of the ill-conditioning problem by means of a series of numerical experiments performed on a representative sample of robot mechanisms. These experiments show how the condition number varies as a function of the number of links in the mechanism,

the relative sizes of the links, the connectivity (characterized by a branching-factor parameter), and a fixed or a floating base. The experiments were conducted on planar, spherical, "circular" and spatial mechanisms, and in a variety of configurations. However, the investigation was limited to kinematic trees containing only revolute joints. The experiments were performed using Matlab.

The main result of this investigation is that the condition number is indeed rather large, even for quite innocuous mechanisms, and that it grows asymptotically with the number of links anywhere from $O(N)$ to $O(N^4)$. For example, a planar mechanism with identical links (as defined in Section 3) has a maximum condition number of approximately $4 N^4$. If there are 40 links in the mechanism, then the condition number can be as high as 10^7, which would make the JSIM numerically singular in 32-bit floating-point arithmetic. If the links are not all the same size, then the condition number can be substantially higher still. On the other hand, branched connectivity and a floating base both tend to reduce the condition number. Even so, the results in this paper suggest that efforts to simulate and control robotic systems with a large number of bodies will be hampered by ill-conditioning to a much greater extent than might be supposed from the relatively good results we currently obtain with typical six-degrees-of-freedom (6-DoF) robots.

Much is already known about the properties of the JSIM, precisely because of its central role in many dynamics and control algorithms, but there does not appear to have been any previous attempt to quantify the ill-conditioning problem. Many properties of the JSIM were investigated by Tourassis and Neuman (1985a, 1985b), but not the condition number. Ghorbel, Srinivasan, and Spong (1998) investigate the boundedness of the eigenvalues of the JSIM, which is an essential prerequisite for the application of some control techniques. They come up with some bounds on the largest and smallest eigenvalue from which an upper limit to the condition number could be deduced. Angeles and Ma (1988) quote figures in the range of 1275–1399 for the condition number of the PUMA 600 over some example trajectories, and figures in the range of 3054–11,934 for the Stanford Arm. They remark that these figures are large enough to cause (significant) round-off

errors in calculations involving the JSIM. Ascher, Pai, and Cloutier (1997) consider the impact of ill-conditioning on the efficiency of the dynamics simulation process. They show that some dynamics algorithms cope better than others, and they suggest a modification to the articulated-body algorithm to improve its performance on ill-conditioned systems. They also mention several examples of robot mechanisms where ill-conditioning can be expected, including systems with long kinematic chains or large differences in link sizes. Featherstone (1999) plots the accuracy of several recursive dynamics algorithms against N. These data show that some algorithms are much more accurate than others, but that they all lose accuracy as N increases. Both the works of Featherstone and of Ascher et al. show that the problem lies with the mechanism itself, since the effect is felt even by algorithms that do not calculate or use the JSIM at any stage.

This paper continues with a short review of the ill-conditioning problem, followed by a description of the robot models used in the experiments, followed by the experiments themselves.

2. Ill-Conditioning

Let $\mathbf{A}$ be a non-singular matrix. The condition number of $\mathbf{A}$, denoted $\kappa(\mathbf{A})$, is a measure of the relative distance from $\mathbf{A}$ to the set of singular matrices (Golub and Van Loan 1989). (Actually, it is the reciprocal of the distance.) It therefore depends on the choice of underlying matrix norm. I have chosen to use the 2-norm in this paper, in which case the condition number is defined as

$$\kappa(\mathbf{A}) = \frac{\sigma_{max}(\mathbf{A})}{\sigma_{min}(\mathbf{A})}$$

where $\sigma_{max}(\mathbf{A})$ and $\sigma_{min}(\mathbf{A})$ are the largest and smallest singular values, respectively, of the matrix $\mathbf{A}$. If $\mathbf{A}$ happens to be symmetric and positive-definite, like the JSIM, then the singular values are the same as the eigenvalues, and the condition number can be given by the alternative definition

$$\kappa(\mathbf{A}) = \frac{\lambda_{max}(\mathbf{A})}{\lambda_{min}(\mathbf{A})}$$

where $\lambda_{max}(\mathbf{A})$ and $\lambda_{min}(\mathbf{A})$ are the largest and smallest eigenvalues of $\mathbf{A}$. If $\kappa(\mathbf{A})$ is large then $\mathbf{A}$ is said to be ill-conditioned.

The condition number of $\mathbf{A}$ defines an upper limit to the loss of precision in computations involving $\mathbf{A}$. Given a system described by the equation

$$\mathbf{y} = \mathbf{A}\,\mathbf{x},$$

the relative error in computing $\mathbf{y}$ from $\mathbf{x}$ is bounded by

$$\frac{\|\boldsymbol{\delta}\mathbf{y}\|}{\|\mathbf{y}\|} \leq \kappa(\mathbf{A})\,\frac{\|\boldsymbol{\delta}\mathbf{x}\|}{\|\mathbf{x}\|},$$
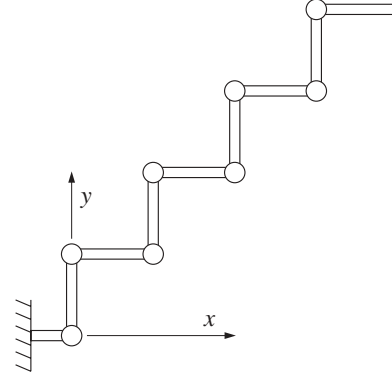

Fig. 1. An eight-link planar robot with an ill-conditioned JSIM (actually $hydra(8, 1, 0, 1)$ in configuration $zag(\pi/2)$).

and the relative error in computing $\mathbf{x}$ from $\mathbf{y}$ is bounded by

$$\frac{\|\boldsymbol{\delta}\mathbf{x}\|}{\|\mathbf{x}\|} \leq \kappa(\mathbf{A}^{-1})\,\frac{\|\boldsymbol{\delta}\mathbf{y}\|}{\|\mathbf{y}\|} = \kappa(\mathbf{A})\,\frac{\|\boldsymbol{\delta}\mathbf{y}\|}{\|\mathbf{y}\|}$$

(since $\kappa(\mathbf{A}) = \kappa(\mathbf{A}^{-1})$), where $\boldsymbol{\delta}\mathbf{x}$ and $\boldsymbol{\delta}\mathbf{y}$ satisfy

$$\mathbf{y} + \boldsymbol{\delta}\mathbf{y} = \mathbf{A}\,(\mathbf{x} + \boldsymbol{\delta}\mathbf{x}).$$

The larger the value of $\kappa(\mathbf{A})$, the greater the potential for loss of accuracy.

The practical significance of ill-conditioning can be illustrated with a simple example. Suppose we wish to command the planar robot shown in Figure 1 to accelerate from rest with a desired joint acceleration vector of

$$\ddot{\mathbf{q}}_d = [1, 1, 1, 1, 1, 1, 1, 1]^{\mathrm{T}}.$$

The equation of motion for this robot is

$$\boldsymbol{\tau} = \mathbf{H}(\mathbf{q})\,\ddot{\mathbf{q}} + \mathbf{C}(\mathbf{q}, \dot{\mathbf{q}})$$

where $\boldsymbol{\tau}$ is the joint force vector, $\mathbf{q}$ and $\dot{\mathbf{q}}$ are the joint position and velocity vectors, $\mathbf{H}(\mathbf{q})$ is the JSIM, and $\mathbf{C}(\mathbf{q}, \dot{\mathbf{q}})$ is the sum of the gravity, Coriolis, and centrifugal terms. However, as this robot moves in a horizontal plane (no gravity terms), and is initially at rest ($\dot{\mathbf{q}} = \mathbf{0}$), the term $\mathbf{C}(\mathbf{q}, \dot{\mathbf{q}})$ simplifies to zero in this particular instance. The exact value of $\boldsymbol{\tau}$ required to produce $\ddot{\mathbf{q}}_d$ is therefore

$$\boldsymbol{\tau}_d = \mathbf{H}\,\ddot{\mathbf{q}}_d = \begin{bmatrix} 302.0450\cdots \\ 250.2104\cdots \\ \vdots \\ 8.6767\cdots \end{bmatrix}.$$

If we apply exactly $\boldsymbol{\tau}_d$ to the robot then we will obtain the desired response; but what happens if we apply a slightly

different force? Suppose the actuators are slightly imperfect, so that the actual applied force, $\boldsymbol{\tau}_a$, differs very slightly from $\boldsymbol{\tau}_d$. Let us say that $\boldsymbol{\tau}_a$ is $\boldsymbol{\tau}_d$ rounded to three significant figures. The robot's response to $\boldsymbol{\tau}_a$ will be

$$\ddot{\mathbf{q}}_a = \mathbf{H}^{-1}\boldsymbol{\tau}_a = \mathbf{H}^{-1}\begin{bmatrix} 302 \\ 250 \\ 201 \\ 151 \\ 106 \\ 64.5 \\ 31.5 \\ 8.68 \end{bmatrix} = \begin{bmatrix} 0.7917 \\ 1.0281 \\ 1.4904 \\ 0.6886 \\ 1.1026 \\ 1.0911 \\ 0.5626 \\ 1.2384 \end{bmatrix}. \quad (1)$$

The actual response is very different from the desired response, with errors of up to 50% on individual joint axes, and yet the applied forces were all accurate to better than 0.5%. High sensitivity to changes in inputs or parameters is a characteristic property of ill-conditioned systems.

In this example, the relative error was magnified by a factor of about 100; but $\kappa(\mathbf{H}) \simeq 1500$ in the configuration shown, and there are other configurations where $\kappa(\mathbf{H}) > 10,000$, so the mechanism is capable of exhibiting far greater sensitivity than was evident in this one example.

The acceleration errors lie predominantly in a subspace of joint motions that cause the least movement of the bodies in the robot mechanism. This raises the question of whether this is indeed an important effect, or something that can be ignored. In a simulation context, these are the fast modes of a stiff system, and therefore cannot be ignored. In a control context, the answer is less clear. It probably depends on how the control system works. Any control system that uses an inverse dynamics calculation to linearize the plant is likely to be adversely affected.

Another point to note is that the problem lies with the robot itself, not just the JSIM. Equation (1) gives an accurate value for the acceleration response to an applied force of $\boldsymbol{\tau}_a$; and the result would not be any different if the computation were performed in a manner that bypassed the calculation and use of the JSIM (e.g., by using the articulated-body algorithm). So it is fair to say that the mechanism itself is ill-conditioned in some sense, and that the condition number of the JSIM is a manifestation of this physical property rather than a purely numerical artifact.

Having put forward the idea that a rigid-body system can be ill-conditioned, it is natural to ask what exactly this means, and how it can be quantified. Unfortunately, there is no easy answer to these questions. The obvious way to proceed is to define the condition number of a mechanism at a specified configuration to be the ratio of the largest and smallest responses to an applied force of unit magnitude at that configuration. The problem with this definition is that there is no natural metric on the space of generalized forces, and likewise no natural metric on the space of generalized accelerations. Without appropriate metrics, one cannot define what is

meant by a unit force or the ratio of the magnitudes of two accelerations.

It is possible to proceed by defining an artificial metric. Only one metric is required because a metric defined on one space will induce a metric on the other. In the general case, a mechanism can contain both revolute and prismatic joints; so an artificial metric must answer the question of how many radians of rotation shall be considered equal in magnitude to a displacement of one meter. I have chosen to avoid this issue by excluding mechanisms containing non-revolute joints. The artificial metric used in this paper is a Euclidean metric in a system of joint coordinates such that the unit acceleration is one radian per second per second and the unit force is one Newton meter. (One must specify the units as the JSIM is not invariant w.r.t. a change of units.) The final experiment in this paper compares this metric with an inertia-weighted metric.

The main difficulty with using an artificial metric is that the eigenvalues and eigenvectors of the JSIM depend on the choice of metric. This is because the JSIM represents a mapping from one vector space to another. The standard formula for defining eigenvalues and eigenvectors is

$$\mathbf{A}\mathbf{x} = \lambda\mathbf{x}, \quad (2)$$

but this formula assumes that $\mathbf{A}$ is a mapping of a vector space into itself, i.e., $\mathbf{A} : U \mapsto U$ where U is a vector space. If, instead, $\mathbf{A}$ is a mapping from one vector space to another, e.g. $\mathbf{A} : U \mapsto V$, then eq. (2) cannot be used because the left-hand side is an element of V, the right-hand side is an element of U, and the two cannot be equated. One must instead use the more general formula

$$\mathbf{A}\mathbf{x} = \lambda\mathbf{B}\mathbf{x} \quad (3)$$

where $\mathbf{B}$ is a mapping of the same kind as $\mathbf{A}$. The problem with eq. (3) is that λ and $\mathbf{x}$ are now clearly functions of both $\mathbf{A}$ and $\mathbf{B}$ rather than $\mathbf{A}$ alone. If we use eq. (3) to define the eigenvalues and eigenvectors of the JSIM then the value of $\mathbf{B}$ is determined by the choice of artificial metric. For the metric used in this paper, $\mathbf{B}$ is an identity matrix in joint coordinates. This means we can use eq. (2) for the numerical determination of eigenvalues and eigenvectors.

3. Robot Models

The experiments reported in this paper were carried out using two parametric families of robot mechanisms. For identification purposes, one is called *hydra* and the other is called *onion*. Both consist of tree-structured rigid-body systems with revolute joints and a fixed base. There are four parameters altogether, and they have the same meanings in both families: N is the number of bodies, B is the branching factor, α is the angle between successive joint axes, and ρ controls the relative sizes of the links. For convenience, we use the following notation to refer to these robots: $hydra(N, B, \alpha, \rho)$ means the set of
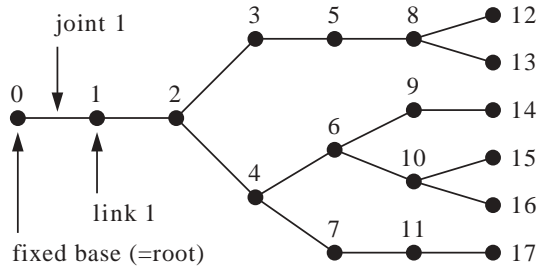
Fig. 2. A kinematic tree with a branching factor of 1.5.

Fig. 3. Link 1 of $hydra(N, B, \alpha, \rho)$.

all hydra robots; $onion(N, 1, 0, 1)$ means the set of all onion robots in which $B = 1$, $\alpha = 0$ and $\rho = 1$; $hydra(33, 1, 0, 1)$ refers to a specific robot; and so on.

The connectivity of a hydra or onion mechanism is defined as follows. First, the fixed base serves as the root of the kinematic tree, and is identified as link number zero. The moving links are then numbered consecutively from 1 to N. The connectivity is described by a body connection array, P, such that $P(i)$ is the link number of the parent of link i. Finally, the joints are numbered such that joint i connects from link $P(i)$ to link i.

P is computed from the branching factor according to the formula

$$P(i) = \lfloor (i - 2 + \lceil B \rceil)/B \rfloor,$$

where the operators $\lfloor \cdots \rfloor$ and $\lceil \cdots \rceil$ round the enclosed expressions down and up, respectively, to the nearest integer. This formula produces a kinematic tree in which the root node has exactly one child, but the other non-terminal nodes have an average of B children each. If $B = 1$, then $P(i) = i - 1$ and the result is an unbranched kinematic chain. If $B = 2$, then $P = [0, 1, 1, 2, 2, \dots]$ and the result is a binary tree. If B is not an integer, then the non-terminal nodes alternate between $\lfloor B \rfloor$ and $\lceil B \rceil$ children in the correct ratio for the average to be B. For example, if $B = 1.5$, then one half of the non-terminals have one child and the other half have two (see Figure 2). A tree constructed according to this formula has minimum depth for the given parameters, but is not necessarily balanced.

The skew parameter, α, is the angle between a link's inboard and outboard joint axes, measured about the common perpendicular from the inboard axis to the outboard axis. This angle is the same for every link in the mechanism. The inboard axis is the one used by the inboard joint, which is the joint that connects the link to its parent. The outboard axis is used by the outboard joints, if any, which connect the link to its children. The base link is a special case: it does not have an inboard axis, and its outboard axis coincides with the z-axis of base coordinates. If a link has more than one child, then it has more than one outboard joint, but they all use the same axis. If $\alpha = 0$, then every axis in the mechanism is parallel.
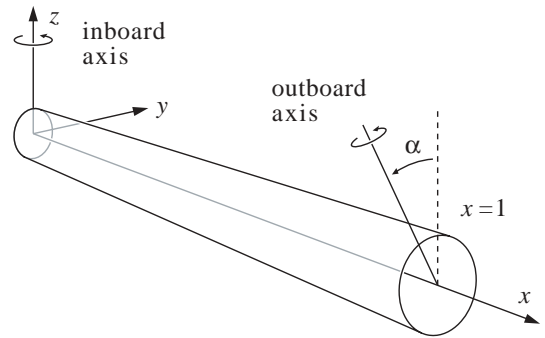
The tapering parameter, ρ, specifies a size ratio between consecutively-numbered links: the length parameters of link $i + 1$ are those of link i multiplied by ρ; the mass of link $i + 1$ is ρ^3 times that of link i; and the rotational inertia of link $i + 1$ is ρ^5 times that of link i. These ratios are consistent with link $i + 1$ being scaled geometrically with respect to link i while keeping the density constant. If $\rho = 1$, then every link in the mechanism is identical.

$hydra(N, B, \alpha, \rho)$ is a family of spatial robots that simplify to planar robots when $\alpha = 1$. Link 1 of a hydra robot is modeled as a thin-walled cylindrical tube of length 1 m and radius 0.05 m (see Figure 3). The tube is centered on the x-axis of the link's local coordinate frame, and it lies between $(0,0,0)$ and $(1,0,0)$ in local coordinates. The inboard joint axis coincides with the local z-axis; and the x-axis of Link 1 coincides with the x-axis of base coordinates when $q_1 = 0$. The outboard joint axis passes through the point $(1,0,0)$ in the direction $(0, -\sin(\alpha), \cos(\alpha))$. The link has a mass of 1 kg, a center of mass at $(0.5,0,0)$, and a rotational inertia about its center of mass of $\mathrm{diag}(0.0025, 1.015/12, 1.015/12)$. The kinematic and inertia properties of the other links are those of Link 1 scaled according to the tapering formulae.

$onion(N, B, \alpha, \rho)$ is a family of spherical robots: every joint axis passes through a single point at the origin of base coordinates, so every link is constrained to rotate about this one point. One possible implementation of an onion robot is shown in Figure 4. If $\alpha = 0$, then every joint axis is coincident with the z-axis of base coordinates, and the links are therefore constrained to rotate about this one axis. This type of mechanism does not appear to have an official name, so I will call them "circular" mechanisms, in analogy with planar and spherical mechanisms. The links of an onion robot are spherically symmetric: their centers of mass lie at the origin, and their rotational inertias are characterized by a single scalar. Link 1 has a rotational inertia of 1 kg m². It is also assigned a mass of 1 kg, but the link mass parameter is unimportant, as it does not affect the equation of motion of this class of robots. The inertia parameters of the other links are calculated via the tapering formulas above.
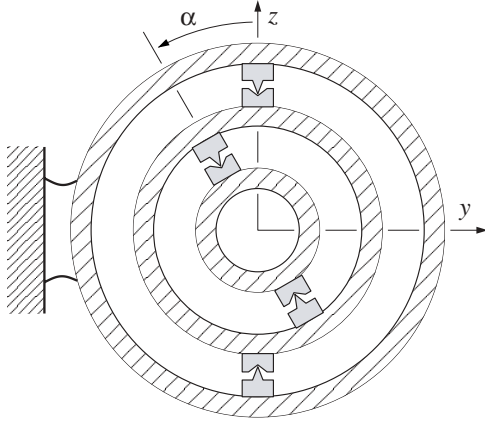
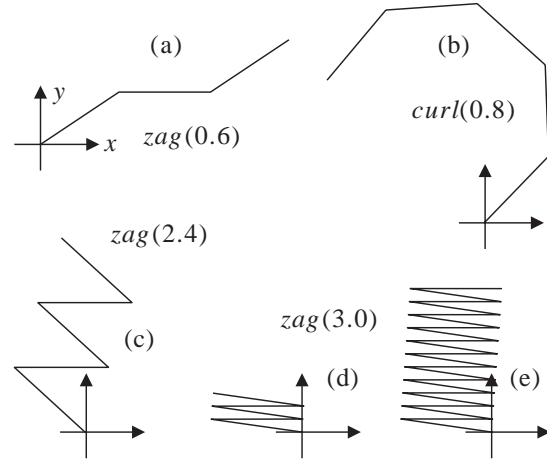Fig. 4. A physical realization of *onion*$(2, 1, \alpha, \rho)$.

Fig. 5. Examples of *zag* and *curl* configurations for robots in the set *hydra*$(N, 1, 0, 1)$. $N = 3$ in (a), $N = 5$ in (b,c,d) and $N = 22$ in (e).

These two families were designed to give a broad coverage of several classes of mechanism while keeping the number of parameters small. They allow us to examine spatial, planar, spherical, and circular mechanisms, branched and unbranched kinematic chains, and systematic variations in link sizes and inertias.

4. Results

This section presents the results of a series of numerical experiments to investigate the condition number, eigenvalues, and eigenvectors of the JSIM of a large sample of hydra and onion robot mechanisms. The experiments were performed using Matlab.

4.1. Unbranched Planar Robots

Let us start with an investigation of how $\kappa(\mathbf{H})$ varies with N for *hydra*$(N, 1, 0, 1)$. These are unbranched planar robots with identical links. To conduct this investigation, we need a means of comparing values of $\kappa(\mathbf{H})$ for robots with different numbers of bodies. The problem is that $\kappa(\mathbf{H})$ depends on $\mathbf{q}$, so a meaningful comparison is only possible if the robots are placed in comparable configurations. Given that we are dealing with configurations of hydra and onion robots, whose configuration spaces vary systematically with N, the following definition is appropriate: two configurations $\mathbf{p} \in \mathsf{R}^m$ and $\mathbf{q} \in \mathsf{R}^n$ ($m < n$) are comparable if $p_i = q_i$ for $i = 1 \ldots m$ and $q_{m+1} \ldots q_n$ follow in a systematic way from $p_1 \ldots p_m$. (Other definitions are possible.)

The experiments in this paper use two parametrized families of comparable configurations, defined as follows:

$$zag(\theta): \ q_i = (-1)^{i+1} \theta, \ \ i = 1 \ldots N$$

and

$$curl(\theta): \ q_i = \theta, \ \ i = 1 \ldots N.$$

Their names were chosen for their effect on planar hydra robots: $zag(\theta)$ puts them into a zigzag shape, and $curl(\theta)$ winds them around a circle. Some examples are shown in Figures 5 and 1. Two robots are in comparable configurations if they are both in $zag(\theta)$ configurations with the same value of θ, or are both in $curl(\theta)$ configurations with the same value of θ. Note that $zag(0) = curl(0)$ and $zag(\pi) = curl(\pi)$. Note also that none of these configurations is singular from a dynamics point of view. A configuration like $zag(0)$ is a kinematic singularity for a hydra robot, but this singularity appears in the Jacobian, not the equation of motion.

Two experiments were performed, and the results are shown in Figures 6 and 7. The first experiment used $zag(\theta)$ configurations and the second used $curl(\theta)$. The curves connect comparable configurations at different values of N. The sample set for N consists of the integers $1 \ldots 8$ followed by values from the E12 series (10, 12, 15, 18, 22, ...) up to 560.

Perhaps the first thing to observe is simply the magnitude of the condition number. It is already up to 44 for a 2-DoF robot, 306 for a 3-DoF robot, and over 40,000 for a 10-DoF robot. A matrix can be considered numerically singular if its condition number is close to the resolution limit of the machine arithmetic. By this measure, the JSIM is already potentially singular in single-precision IEEE floating-point arithmetic at $N = 40$. (The corresponding figure for double-precision arithmetic is $N \simeq 6000$.)

One obvious feature of the curves is that their straight sections have only two slopes. The steeper slope corresponds to a
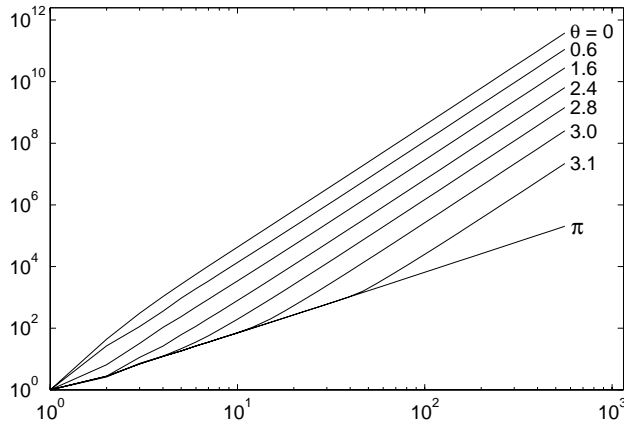
Fig. 6. Condition number of $hydra(N, 1, 0, 1)$ versus N in $zag(\theta)$ configurations for various θ.
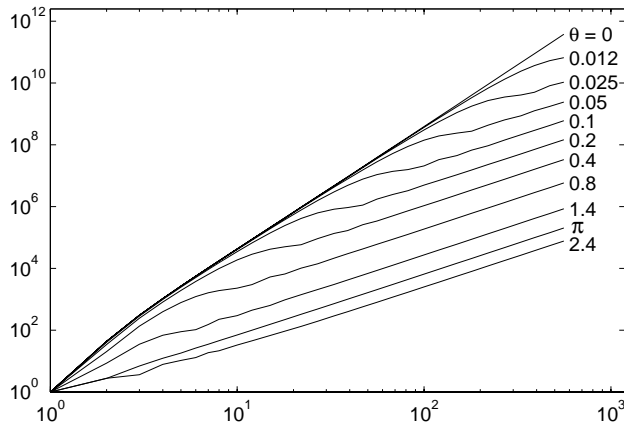

Fig. 7. Condition number of $hydra(N, 1, 0, 1)$ versus N in $curl(\theta)$ configurations for various θ.

fourth-power relationship between condition number and N, i.e., $\kappa(\mathbf{H}) = O(N^4)$, and the shallow slope corresponds to a second-power relationship, $\kappa(\mathbf{H}) = O(N^2)$. An approximate formula for the worst case is $\kappa_{max}(\mathbf{H}) \simeq 4 N^4$.

In Figure 6 the shallow slope is only evident at values of θ approaching π, and there is a fairly sharp transition from the shallow slope to the steep one at a value of N that increases as θ gets closer to π. It turns out that the transition occurs when the zigzag shape formed by the robot covers an area that is approximately square in outline. This happens when $N \simeq \sec(\theta/2)$. In the case of $\theta = 3.0$, for example, the transition occurs at $N = 14$. If $N < 14$, as in Figure 5(d), then the zigzag is wider than it is long; and if $N > 14$, as in Figure 5(e), then the zigzag is longer than it is wide.

This suggests that the composite-rigid-body inertia—the inertia that a specified collection of rigid bodies would have

if they were rigidly connected together to form a single composite rigid body (Featherstone 1987, Section 5.3)—of the robot as a whole is one of the factors in the relationship between $\kappa(\mathbf{H})$ and N. At values of N below the transition, the robot is gaining mass in linear proportion to N. However, its geometrical extent, and hence also its radius of gyration, are dominated by the width of the zigzag, which is not varying with N. At values of N above the transition, the geometrical extent is dominated by the length of the zigzag, which grows linearly with N, so the radius of gyration also grows approximately linearly with N. Thus, the rotational inertia of the whole mechanism grows in proportion to N below the transition, and in proportion to N^3 above the transition.

This hypothesis is supported by the results in Figure 7. In this figure, the steep slope is only evident at small values of θ, and the curves start out with the steep slope and make a transition to the shallow slope. The transition is less sharp, and is followed by a decaying undulation before the curve settles down to the shallow slope. What is happening here is that the mechanism curls into a circular arc of radius approximately $1/\theta$. As N increases, the arc progresses around the perimeter of the circle, and becomes a complete circle when $N \simeq 2\pi/\theta$. The transition begins as the arc approaches a semicircle, and the slope reaches its first minimum when the arc has traced slightly more than one complete circle. Thus, at low values of N, the radius of gyration is growing approximately linearly with N, but, at higher values, it reaches an upper limit determined by the radius of the circle.

4.2. Unbranched Spatial Robots

Are the results of Section 4.1 general, or are they a special property of planar robots? To find out, the first experiment was repeated using the spatial robot family $hydra(N, 1, 0.5, 1)$. These robots adopt a twisted zigzag posture in $zag(\theta)$ configurations that resembles the planar zigzag of $hydra(N, 1, 0, 1)$, but twisted uniformly about its central longitudinal axis. The twisted zigzag is contained within a cylindrical volume with length and diameter equal to the length and width of the corresponding planar zigzag.

Figure 8 shows the results of this experiment alongside the equivalent results for $hydra(N, 1, 0, 1)$. As can be seen, the condition numbers of the spatial robots are slightly lower than their planar counterparts, but the overall asymptotic and transitional behavior is essentially the same. The condition numbers of the spatial robots are smaller by a factor of up to 2.5 on the $O(N^4)$ curves, and only marginally smaller on the $O(N^2)$ curve.

There are two plausible explanations for this result, but they have not been investigated. The first is that the cross-coupling between revolute joints is greatest when their axes are parallel, so one would expect the amount of cross-coupling to be less for a spatial robot than a planar one. The second is that the twisted zigzag is slightly shorter than the planar zigzag when
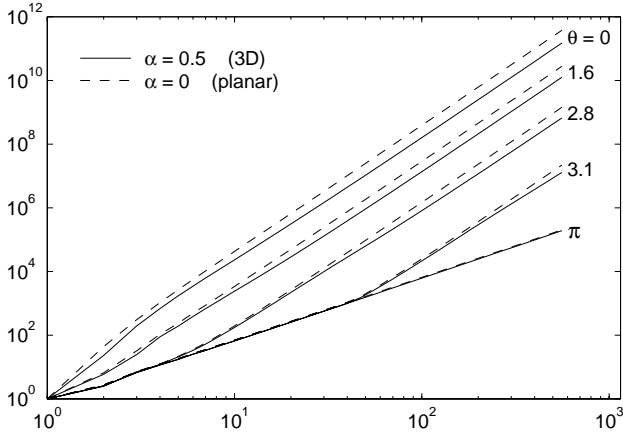
Fig. 8. Condition number of $hydra(N, 1, 0.5, 1)$ versus N in $zag(\theta)$ configurations for various θ.
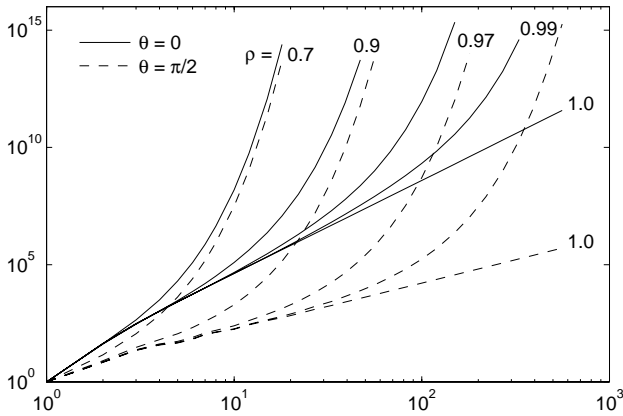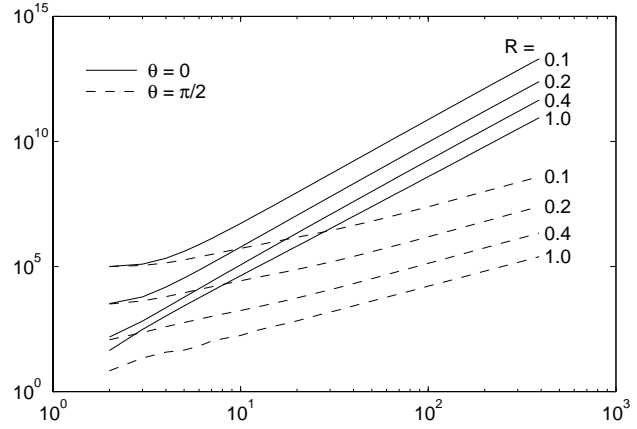

Fig. 10. Condition number of $hydra(N, 1, 0, \rho)$ versus N at $curl(0)$ and $curl(\pi/2)$ configurations for various fixed ratios of largest to smallest link. $\rho = \sqrt[N-1]{R}$.

Fig. 9. Condition number of $hydra(N, 1, 0, \rho)$ versus N at $curl(0)$ and $curl(\pi/2)$ configurations for various values of ρ.

$0 < \theta < \pi$, so its rotational inertia will be slightly less when N is above the transition. The former applies to spatial robots in general, but the latter is specific to this experiment.

4.3. Varying the Link Sizes

Having established that the results of Section 4.1 apply to spatial robots as well as planar, the next step is to vary the link sizes. It is already known from earlier work that a large disparity in link sizes can produce an ill-conditioned JSIM (Ascher, Pai, and Cloutier 1997), but we will examine how link size ratios and N together affect the condition number.

The tapering parameter, ρ, allows us to construct robot mechanisms in which the link sizes follow a geometric progression: the size of link i is that of link $i - 1$ scaled by

ρ. For any fixed value of ρ other than 1, the size ratio between the largest and smallest links grows exponentially with N; so we would expect the size-ratio effect to dominate all others at sufficiently high values of N. This is borne out by the results in Figure 9, which shows the condition number of $hydra(N, 1, 0, \rho)$ plotted against N for various values of ρ in configurations $curl(0)$ and $\text{curl}(\pi/2)$. The curves for $\rho = 0.7$ end at a size ratio of approximately $600 : 1$, and the curves for $\rho = 0.99$ end at ratios of $28 : 1$ in $curl(0)$ and $280 : 1$ in $curl(\pi/2)$. The curves stop just before the JSIM goes singular (in double-precision arithmetic).

A more interesting effect is shown in Figure 10. In this experiment, the condition number of $hydra(N, 1, 0, \rho)$ was plotted against N in configurations of $curl(0)$ and $curl(\pi/2)$, exactly as in Figure 9. However, instead of a fixed tapering coefficient, there is a fixed ratio between the smallest and largest links in the mechanism. ρ is therefore a function of N, and it is given by the formula

$$\rho = \sqrt[N-1]{R}$$

where R is the ratio of smallest to largest link size.

The curves are clearly exhibiting approximately the same asymptotic behavior as those in Figure 7. At $N = 2$, the condition number is dominated by the inertia ratio of the two links, which is R^5. As N increases, the curves converge to some extent before becoming approximately parallel. At $N = 390$, which is where the data end, the ratios between the condition numbers for $R = 0.1$ and $R = 1$ are 227.5 in $curl(0)$ and 1587 in $curl(\pi/2)$. The ratios between $R = 0.1$ and $R = 0.2$ are 8.15 in $curl(0)$ and 15.62 in $curl(\pi/2)$. These numbers are suspiciously close to the integers 8 and 16, but I have not pursued this line of inquiry.

It would be nice if we could conclude that the results of Section 4.1 apply also to robots with differing link sizes,
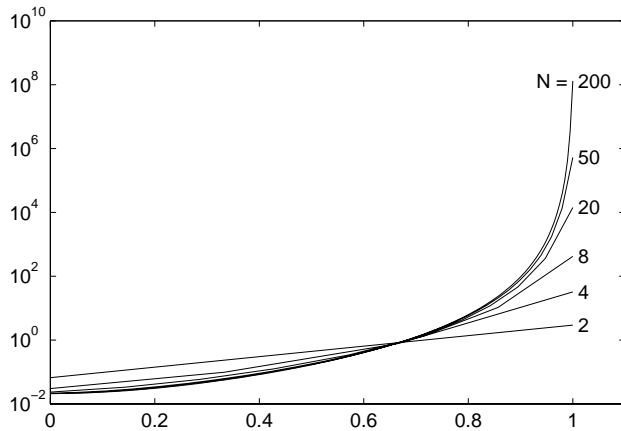
Fig. 11. Eigenvalues of $hydra(N, 1, 0, 1)$ at $zag(0)$, uniformly spread along the x-axis, for various N.
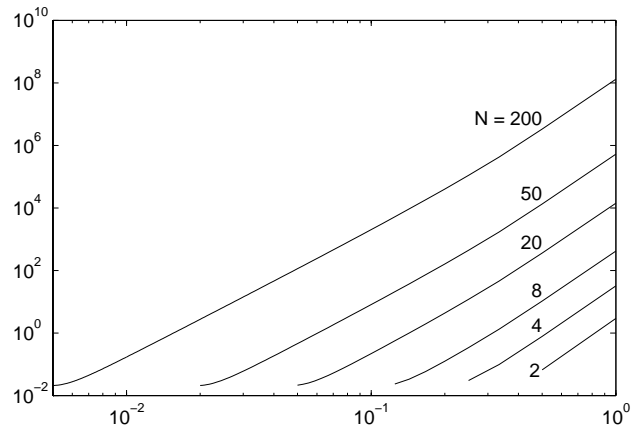

Fig. 12. Eigenvalues of $hydra(N, 1, 0, 1)$ at $zag(0)$ versus normalized period, for various N.

provided the sizes vary within fixed limits. However, the data presented so far are not sufficient to draw such a conclusion, since they relate only to a geometric progression of decreasing link sizes. Other patterns of size variation would have to be investigated.

4.4. Eigenvalues and Eigenvectors

So far, we have only looked at the condition number of the JSIM, which is only a single number. We can get a better picture of the JSIM, and how it varies with N and other parameters, by examining its eigenvalues and eigenvectors.

Figure 11 shows the eigenvalues of $hydra(N, 1, 0, 1)$ in the configuration $zag(0)$ for various values of N. Each curve connects the eigenvalues for one value of N. As there are a different number of eigenvalues in each case, they are spaced uniformly along the x-axis such that the smallest eigenvalue appears at $x = 0$ and the largest at $x = 1$. Thus, the two eigenvalues for the case $N = 2$ appear at $x = 0$ and $x = 1$, the four eigenvalues for the case $N = 4$ appear at $x = 0, 1/3,$ $2/3$ and 1, and so on.

We can see from this figure that the rise in condition number is due to the increasing value of the largest eigenvalue rather than the decreasing value of the smallest. Indeed, the smallest eigenvalue converges to a value of approximately 0.021. This value is configuration-dependent. In zigzag configurations, it varies between a minimum of 0.021 at $zag(0)$ and a maximum of 0.164 at $zag(2.45)$. For comparison, the smallest inertia exhibited by a single link is $I_{min} = 0.08458$, which is its rotational inertia about its center of mass (in the x–y plane); so the smallest eigenvalue of the JSIM is actually smaller than the smallest inertia of a single link by about a factor of 4.

This observation is not just an empirical result. In a few simple cases, it is possible to prove that the smallest eigenvalue

is indeed bounded below by $\lambda_{min} \geq I_{min}/4$. $hydra(N, 1, 0, 1)$ at $zag(0)$ is one such case; $onion(N, 1, 0, 1)$ in any configuration is another.

The curves in Figure 11 also show that most of the eigenvalues are small, and that the larger eigenvalues constitute an ever-smaller proportion of the total as N increases. For example, if we use the geometric mean of the smallest and largest eigenvalues as our threshold, then the proportion of eigenvalues above this threshold dwindles from 50% at $N = 2$ to 5% at $N = 200$.

In Figure 11, the curves appear to be converging everywhere except $x = 1$. This is perhaps a little misleading, since the x scale is different for each curve. Figure 12 presents a clearer picture of how the curves evolve. It shows the same data as Figure 11, but all curves are now plotted on a single x scale such that the ith largest eigenvalue has an x coordinate of $1/i$. Thus, the largest eigenvalue appears at $x = 1$, the second largest at $x = 0.5$, and so on. The result is a series of parallel, nearly-straight lines.

The justification for this scale is as follows. There is a close relationship between the eigenvectors of the JSIM and the vibration modes of the robot. If the eigenvectors are calculated using the Euclidean metric, then they are the same as the vibration modes that the robot mechanism would have if a unit-stiffness torsional spring were to be connected across each joint. If the links are all in a straight line (as they are in $zag(0)$) then the vibration modes consist of a fundamental and a series of harmonics. The eigenvector with the largest eigenvalue is the fundamental; the eigenvector with the second largest eigenvalue is the second harmonic; and so on. Thus, the ith largest eigenvalue can be associated with the ith harmonic, and Figure 12 plots these eigenvalues against their normalized period (the fundamental having a period of 1, the second harmonic a period of 0.5, etc.).
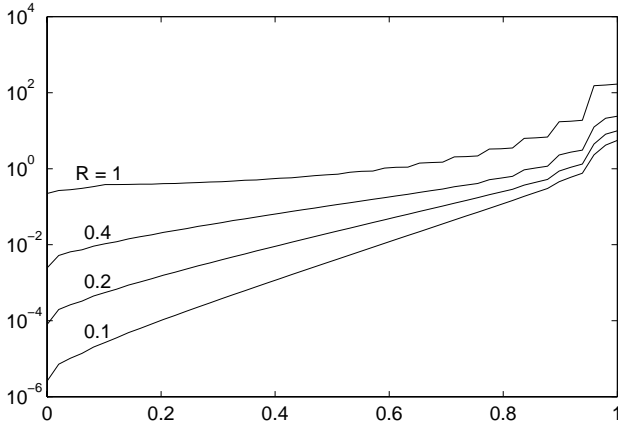
Fig. 13. Effect of tapering on eigenvalues of $hydra(50, 1, 0, \rho)$ at $curl(2.2)$.

Fig. 14. Largest eigenvectors of $hydra(20, 1, 0, 1)$ and $hydra(10, 1, 0, 1)$ at $zag(0)$.

The slope in Figure 12 indicates an approximate fourth-power relationship between eigenvalue magnitude and period. However, the slope would necessarily be different in a configuration where $\kappa(\mathbf{H}) = O(N^2)$, since the value of $\kappa(\mathbf{H})$ is determined by the endpoints of the lines.

This experiment was repeated for various zigzag configurations. The resulting curves differ in scale, and exhibit some irregularities, but are otherwise broadly similar to those in Figure 11. The irregularities can be explained as a manifestation of the more complicated vibration modes that arise in zigzag configurations.

Figure 13 shows an example of a staircase irregularity on the eigenvalue curve, and also shows the effect of tapering. It plots the eigenvalues of $hydra(50, 1, 0, \rho)$ in $curl(2.2)$ for various end-link size ratios (i.e., $\rho = \sqrt[49]{R}$) on the same x scale as for Figure 11. There is nothing special about this configuration: it was chosen simply because it produces a clear example of a staircase. It just so happens that the condition number of $hydra(50, 1, 0, 1)$ is quite low in $curl(2.2)$. However, despite the large difference in scale and the superimposed staircase pattern, the curves for $hydra(50, 1, 0, 1)$ in Figures 13 and 11 do have approximately the same overall shape.

The effect of tapering is to alter the slope of the left and central portions of the curve. It also smooths out the irregularities to some extent. The smallest eigenvalue decreases in proportion to the inertia of the smallest link (i.e., in proportion to R^5); and the largest eigenvalue decreases slightly faster than the composite inertia of the whole mechanism (i.e., slightly faster than H_{11}). Asymptotically, the former dominates. These results provide part of the explanation for the effects seen in Figure 10.

Now let us look at some eigenvectors. Figure 14 shows the three largest eigenvectors of $hydra(20, 1, 0, 1)$ ($\mathbf{e}_1$, $\mathbf{e}_2$ and $\mathbf{e}_3$) and the largest eigenvector of $hydra(10, 1, 0, 1)$ ($\mathbf{d}_1$), all
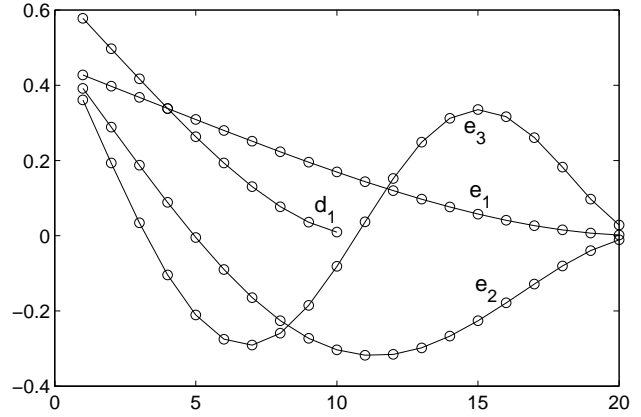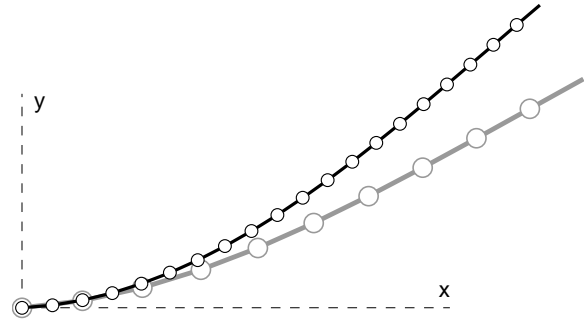

Fig. 15. $hydra(10, 1, 0, 1)$ and $hydra(20, 1, 0, 1)$ in configurations of 0.2 times their largest eigenvectors.

plotted in joint coordinates (i.e., the ith circle on each curve is the joint-i coordinate of the eigenvector). $\mathbf{e}_2$ and $\mathbf{e}_3$ have been included only to illustrate the connection between eigenvalues and vibration modes.

Figure 14 provides us with an explanation of why, in Figures 6 and 7, the condition number grows faster by one power of N than the composite inertia of the whole mechanism. Observe that the coordinates of $\mathbf{d}_1$ and $\mathbf{e}_1$ are all positive. This means that the corresponding joint motions sum along the length of the mechanism. The effect is illustrated in Figure 15, which shows $hydra(10, 1, 0, 1)$ in the configuration $0.2\,\mathbf{d}_1$ and $hydra(20, 1, 0, 1)$ in $0.2\,\mathbf{e}_1$, the two robots being scaled to appear the same size. Observe that $hydra(20, 1, 0, 1)$ has curved more than $hydra(10, 1, 0, 1)$, despite the fact that both vectors have the same Euclidean magnitude. This is because $\sum_{i=1}^{20} e_{1i} > \sum_{i=1}^{10} d_{1i}$ even though $\sum_{i=1}^{20} e_{1i}^2 = \sum_{i=1}^{10} d_{1i}^2 = 1$. In fact, one can show that the sum of the elements of the largest eigenvector grow in proportion to $\sqrt{N}$.
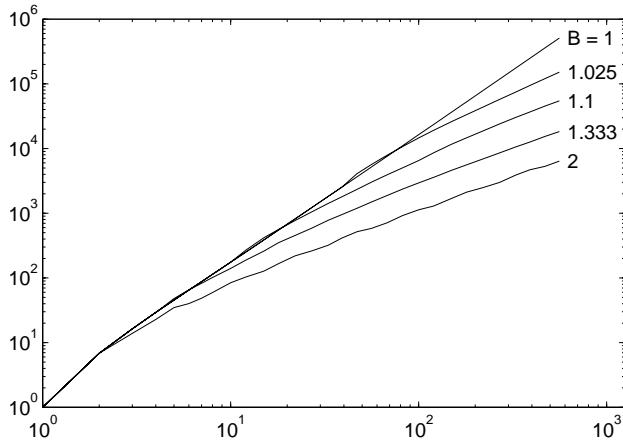
Fig. 16. Condition number of *onion*$(N, B, 0, 1)$ versus N at *curl*(0) for various values of B.

Fig. 17. Largest eigenvectors of *onion*$(33, B, 0, 1)$ for $B = 1$ and $B = 1.125$.

The effect is like having a gear box with a gear ratio of $\sqrt{N}$ interposed between joint space and the mechanism itself: if the actual inertia is growing in proportion to N^x, then the apparent inertia in joint space is growing in proportion to N^{x+1}, being the actual growth multiplied by the square of the gear ratio. As there is no gearing effect on the smallest eigenvalue, the net effect on the condition number is that it too grows by one power of N faster than the composite inertia of the mechanism.

For the mechanisms we have studied so far, the following formula accurately predicts the asymptotic behavior of $\kappa(\mathbf{H})$, but not its magnitude:

$$\kappa(\mathbf{H}) = O(N\, H_{11}/H_{NN}).$$

Essentially, it says that the asymptotic behavior is the product of the gearing effect and the ratio of the largest and smallest inertias in the system. (It assumes that Link N is the smallest link in the mechanism.)

4.5. Branching Factor

Let us now examine the condition number of branched kinematic chains. We shall use onion robots, rather than hydra, on the grounds that altering the branching factor of a hydra robot causes a large change in its shape, and hence its mass distribution. In contrast, the links of an onion robot are all spherically symmetric and centered at the origin; so this family of robots allows us to study the effects of varying the branching factor while keeping the mass distribution constant.

Figure 16 shows how the condition number of *onion*$(N, B, 0, 1)$ varies with N for various values of B. These are circular robots, because the skew angle is set to zero, which means that the condition number is independent of configuration. The curve corresponding to $B = 1$ has a slope that
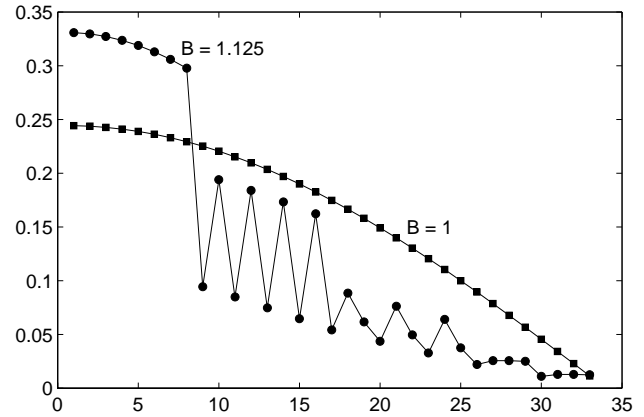
is $O(N^2)$, which is consistent with earlier results. For this class of mechanisms, the composite rigid-body inertia of the whole mechanism grows in proportion to N, so the condition number grows in proportion to N^2.

Branching factors greater than 1 produce curves that follow the $B = 1$ curve up to the point where the first branch occurs, and then make a gradual transition to an approximately $O(N)$ slope. The curves bottom out at $B = 2$, i.e., the curves for $B > 2$ all follow approximately the same path as for $B = 2$. (This was checked up to $B = 4$.)

This experiment was repeated with *onion*$(N, B, 1, 1)$, in order to discover whether the results in Figure 16 apply to spherical robots in general, or are just a special property of circular robots. The curves for *onion*$(N, B, 1, 1)$ are lower in magnitude and slightly more irregular in shape than those for *onion*$(N, B, 0, 1)$; but they follow the same pattern as the curves in Figure 16, except that they bottom out at $B = 3$ instead of $B = 2$.

An explanation for these results can be found in Figure 17. This figure shows the joint-space coordinates of the largest eigenvectors of *onion*$(33, 1, 0, 1)$ and *onion*$(33, 1.125, 0, 1)$. The latter has branch points at links 8, 16 and 24; so the first eight joints all lie on a common stem, the next eight lie alternately in one or other of two subtrees, the next nine each lie in one of three subtrees, and the final eight each lie in one of four subtrees. The individual joint coordinates are clearly weighted according to the number of links supported by the joint: motion is concentrated into the joints that move the largest number of links. The concentration becomes more pronounced as B increases.

Branching diminishes, and eventually eliminates, the gearing effect for two reasons. The first is that the gearing effect depends on the summation of motion that occurs when joints are connected in series. In an unbranched chain, all N joints
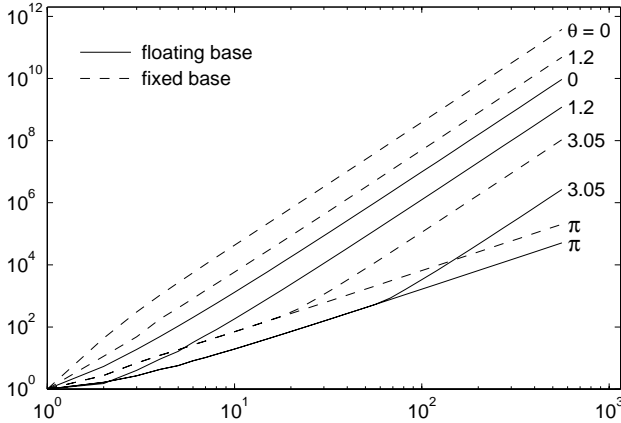
Fig. 18. Condition number of floating-base *hydra* $(N+1, 1, 0, 1)$ compared with fixed-base *hydra*$(N, 1, 0, 1)$ in *zag*(θ) configurations.

Fig. 19. Fixed-base *hydra*$(10, 1, 0, 1)$ and floating-base *hydra*$(11, 1, 0, 1)$ in configurations of 0.2 times their largest eigenvectors.

are connected in series. In a branched chain, the determining factor is the maximum number of joints between any link and the base, which is, of course, given by the depth of the tree. With hydra and onion robots, the depth of the tree grows in proportion to $\log(N)$ when $B > 1$. The second reason is that the gearing effect is largest when a large proportion of the joints contribute almost equally to the motion, and is smallest when a small number of joints account for most of the motion; so the gearing effect is reduced when the motion is concentrated into the joints nearest the root.

4.6. Floating Bases

A floating-base robot is one that does not have a permanent kinematic connection to a fixed location in space. Examples include humanoids, space robots, and mobile robots in general. This category includes many robots with relatively large values of N, so it makes sense to examine the effect of a floating base on the condition number of the JSIM.

The method used here is to compare the condition number of a floating-base robot with its fixed-base equivalent. The latter is obtained from the former by attaching the floating base to a fixed location. A special function was written to convert a fixed-base hydra robot to a floating-base robot by removing the first joint. Starting with $hydra(N, B, \alpha, \rho)$, this function produces a robot with N bodies but only $N-1$ joints. Its fixed-base equivalent is therefore the robot $hydra(N-1, B, \alpha, \rho)$. (There is a scale error in this comparison if $\rho \neq 1$, but the condition number is independent of scale.)

Figure 18 compares $\kappa(\mathbf{H})$ for fixed-base and floating-base $hydra(N, 1, 0, 1)$ in various zigzag configurations. It shows that the condition number behaves in essentially the same manner for a floating-base robot as for a fixed-base robot,
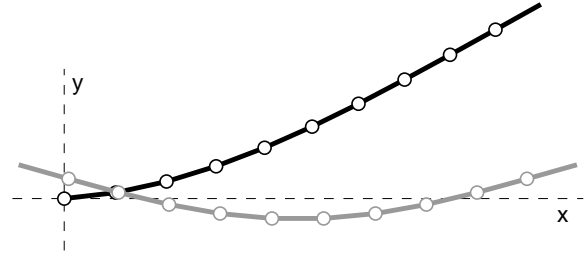
but is somewhat smaller in magnitude. In this particular experiment, the floating-base condition number is a factor of 4 lower on the $O(N^2)$ slopes, a factor of 40 lower on the $O(N^4)$ slopes, and the transition occurs at a value of N approximately a factor of 3 larger than for the fixed-base case.

In general, a floating base will reduce the largest eigenvalue of the JSIM. This will usually lead to a smaller condition number, but not always. Figure 19 compares the largest eigenvectors of fixed-base $hydra(10, 1, 0, 1)$ and floating-base $hydra(11, 1, 0, 1)$. Observe that the latter involves much less movement of mass. This will be true in general, since the overall centre of mass remains stationary in a floating-base system. (The application of external forces is a separate issue.) In this particular example, the floating-base eigenvector produces a symmetrical bend, each half of which resembles the fixed-base bend of a robot with half as many joints. The situation would, of course, be different if the robot were tapered or branched.

Despite the reduction in the largest eigenvalue, it is possible for a floating-base robot to have a larger condition number than its fixed-base equivalent. This happens when the floating-base link plays an important role in determining the smallest eigenvalue. To take an extreme example, consider floating-base $hydra(3, 1, 0, 10)$ in $zag(\pi/2)$. The floating base in this mechanism is the smallest link by a factor of 10, and it determines the magnitude of the smallest eigenvalue. The condition number of this mechanism is 10^5; but the condition number of its fixed-base equivalent is only 136, mainly because of a large increase in the smallest eigenvalue.

4.7. Changing the Metric

All of the results so far have been obtained using a Euclidean metric. One obvious criticism of this approach is that the Euclidean metric treats all joints equally. This is difficult to justify when one considers that some joints have a much larger effect than others on the motion of the mechanism. This section repeats some of the earlier experiments, and compares

the results obtained using the Euclidean metric with those obtained using an inertia-weighted metric.

Suppose we define a new unit of rotational measure individually for each joint, so that rotation about joint i is measured in units of $d_i \times$ radians, where d_i is a scaling factor. It is then necessary to adjust the units of joint force so that a unit force about joint i is $1/d_i$ Newton meters. This adjustment preserves the correct relationship between generalized motion coordinates and generalized force coordinates. If $\ddot{\mathbf{q}}$, $\boldsymbol{\tau}$, and $\mathbf{H}$ represent a joint acceleration vector, a joint force vector, and a JSIM in the original coordinates, and $\ddot{\mathbf{q}}'$, $\boldsymbol{\tau}'$, and $\mathbf{H}'$ represent the same quantities in the new coordinates, then

$$\ddot{\mathbf{q}}' = \mathbf{D}^{-1}\,\ddot{\mathbf{q}}\,, \qquad \boldsymbol{\tau}' = \mathbf{D}\,\boldsymbol{\tau}$$

and

$$\mathbf{H}' = \mathbf{D}\,\mathbf{H}\,\mathbf{D},$$

where

$$\mathbf{D} = \mathrm{diag}(d_1, d_2, \ldots, d_N)$$

(a diagonal matrix). If we choose d_i according to the formula

$$d_i = H_{ii}^{-0.5}$$

then the diagonal elements of $\mathbf{H}'$ are all unity. Thus, $\mathbf{D}$ is the coordinate transformation matrix that scales the units of measurement in joint space such that each joint sees a unit inertia. The Euclidean metric in this scaled coordinate system is equivalent to an inertia-weighted metric in the original coordinates; so, if we define $\kappa'(\mathbf{H})$ to be the condition number of $\mathbf{H}$ according to the inertia-weighted metric, then

$$\kappa'(\mathbf{H}) = \kappa(\mathbf{H}') = \kappa(\mathbf{D}\,\mathbf{H}\,\mathbf{D}).$$

Figure 20 shows both $\kappa(\mathbf{H})$ and $\kappa'(\mathbf{H})$ for $hydra(N, 1, 0, 1)$ in $zag(\theta)$ configurations for various values of θ. Overall, the two metrics produce very nearly the same results. The inertia-weighted metric produces slightly smaller condition numbers at low values of N and slightly larger condition numbers at large values of N.

This is an interesting result because it demonstrates that the well-known large differences in magnitude between the largest and smallest diagonal elements of $\mathbf{H}$ are not the cause of the ill-conditioning problem: if one scales the matrix to make all the diagonal elements the same, then the condition number goes up, not down, for large N.

Figure 21 shows $\kappa(\mathbf{H})$ and $\kappa'(\mathbf{H})$ for $hydra(N, 1, 0, \rho)$ in $curl(0)$ for various values of ρ. The two metrics are now clearly producing very different results: for $\rho < 1$, $\kappa(\mathbf{H})$ grows exponentially with N, while $\kappa'(\mathbf{H})$ converges to a limit that depends on ρ.

There are not enough data here to draw any firm conclusions, but it does suggest the following physically-plausible
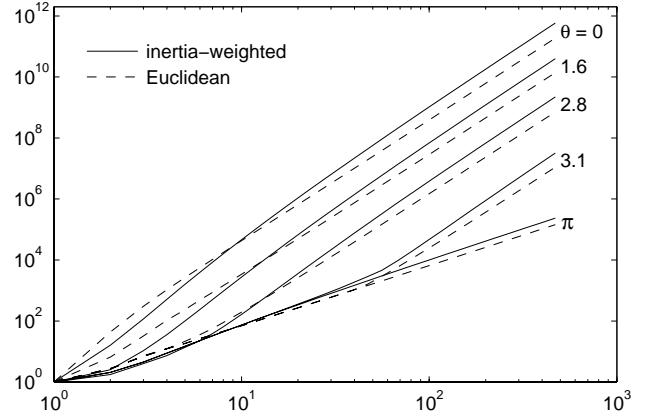

Fig. 20. Condition number of $hydra(N, 1, 0, 1)$ according to both the inertia-weighted and Euclidean metrics, in $zag(\theta)$ configurations for various θ.

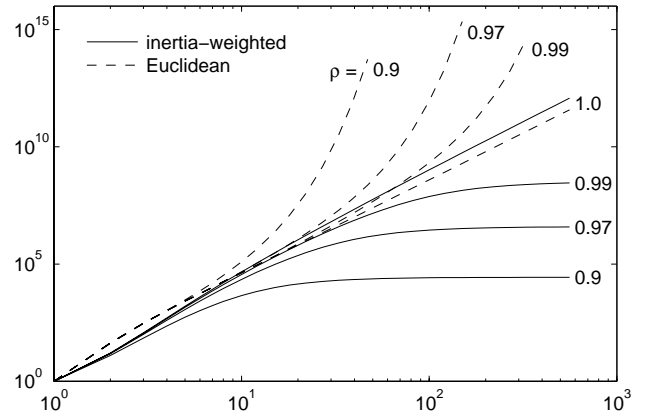Fig. 21. Condition number of $hydra(N, 1, 0, \rho)$ according to both the inertia-weighted and Euclidean metrics, at $curl(0)$, for various values of ρ.

hypothesis: the ill-conditioning of the underlying mechanical system is caused largely by dynamic interactions between the bodies; the effect is strongest when the bodies have similar inertias; and it diminishes to zero as the inertia differences grow. This would imply that κ' is providing a reasonable indication of the underlying ill-conditioning when $\rho < 1$, while κ is providing an overestimate.

Additional support for this hypothesis comes from examining the elements of $\mathbf{H}'$. For example, for $hydra(5, 1, 0, \rho)$ in $curl(0)$, we have

$$\mathbf{H}' = \begin{bmatrix} 1 & 0.984 & 0.929 & 0.822 & 0.625 \\ 0.984 & 1 & 0.974 & 0.884 & 0.687 \\ 0.929 & 0.974 & 1 & 0.952 & 0.769 \\ 0.822 & 0.884 & 0.952 & 1 & 0.883 \\ 0.625 & 0.687 & 0.769 & 0.883 & 1 \end{bmatrix}$$

when $\rho = 1$, and

$$\mathbf{H}' = \begin{bmatrix} 1 & 0.594 & 0.252 & 0.097 & 0.034 \\ 0.594 & 1 & 0.593 & 0.251 & 0.092 \\ 0.252 & 0.593 & 1 & 0.590 & 0.238 \\ 0.097 & 0.251 & 0.590 & 1 & 0.559 \\ 0.034 & 0.092 & 0.238 & 0.559 & 1 \end{bmatrix}$$

when $\rho = 0.5$. The off-diagonal elements H'_{ij} measure the dynamic interaction between bodies i and j. These values are all lower when $\rho = 0.5$, and their magnitudes diminish as the size difference between bodies i and j increases. $\mathbf{H}'$ converges to the identity matrix as $\rho \to 0$.

5. Conclusion

This paper has presented an empirical study of the condition number of the JSIM, backed up with some investigation of the eigenvalues and eigenvectors of the JSIM. The study was restricted to two families of robots in which all the joints were revolute, but it included examples of planar, spatial, spherical, and "circular" robots, systematic variations in relative link sizes, branched and unbranched chains, and both fixed and floating bases. Condition numbers were calculated using two families of comparable configurations: one in which all the joint angles were the same, and one in which they alternated in sign.

The general conclusion one can draw from this study is that the condition number can be very large, and it can grow asymptotically with the fourth power of the number of bodies in the system. For a simple planar chain of identical links, the maximum condition number is approximately $4N^4$, where N is the number of bodies. Thus, a chain of only 10 links already can exhibit a condition number of 40,000.

If the link sizes vary, then the condition number of the JSIM goes up as the size differences increase. However, if the JSIM is first scaled to have unit elements along the diagonal, then the condition number of this scaled matrix goes down as the size differences increase. Branches in the kinematic chain can reduce the growth in the condition number by up to one power of N compared with an unbranched chain. A floating base can make matters worse, but typically yields a modest reduction in condition number that does not appear to grow with N.

The significance of these results is that ill-conditioned systems are both harder to simulate accurately and harder to control. Although a typical 6-DoF robot arm can be simulated and controlled perfectly adequately, this does not mean that the same would necessarily be true of a larger system, since the condition number grows so rapidly with N. This is not just a problem with the JSIM. It is a physical property of the robot mechanism, and will therefore have an effect even on simulators and control systems that do not use the JSIM.

Finally, all the results in this paper depend on an arbitrary choice of metric. Only two metrics were investigated: a Euclidean metric in a configuration space of revolute joint angles, and an inertia-weighted version of the Euclidean metric. A different choice of metric may well produce different results.

References

Angeles, J., and Ma, O. 1988. Dynamic simulation of n-axis serial robotic manipulators using a natural orthogonal complement. *International Journal of Robotics Research* 7(5):32–47.

Ascher, U. M., Pai, D. K., and Cloutier, B. P. 1997. Forward dynamics, elimination methods, and formulation stiffness in robot simulation. *International Journal of Robotics Research* 16(6):749–758.

Featherstone, R. 1987. *Robot Dynamics Algorithms*. Kluwer Academic, Boston, MA.

Featherstone, R. 1999. A divide-and-conquer articulated-body algorithm for parallel $O(\log(n))$ calculation of rigid-body dynamics. Part 2: trees, loops and accuracy. *International Journal of Robotics Research* 18(9):876–892.

Ghorbel, F., Srinivasan, B., and Spong, M. W. 1998. On the uniform boundedness of the inertia matrix of serial robot manipulators. *Journal of Robotic Systems* 15(1):17–28.

Golub, G. H. and Van Loan, C. F. 1989. *Matrix Computations*. Johns Hopkins University Press, Baltimore, MD.

Tourassis, V. D. and Neuman, C. P. 1985a. Properties and structure of dynamic robot models for control engineering applications. *Mechanism and Machine Theory* 20(1):27–40.

Tourassis, V. D. and Neuman, C. P. 1985b. The inertial characteristics of dynamic robot models. *Mechanism and Machine Theory* 20(1):41–52.